Experimental validation of a compact mixed-flow compressor for an active high-lift system

IOP Conf. Series: Materials Science and Engineering **643** (2019) 012142 doi:10.1088/1757-899X/643/1/012142

Experimental validation of a compact mixed-flow compressor for an active high-lift system

Felix Kauth[1,*], Niklas Maroldt[1], and Joerg R Seume[1]

[1] Leibniz University, Institute of Turbomachinery and Fluid Dynamics, 30167 Hannover, Germany

[*] E-mail: kauth@tfd.uni-hannover.de

Abstract. Compact, electrically-driven compressors are a core component of a novel active high-lift system for future commercial aircraft. A newly-developed aeromechanical optimization process was used to design the compressor stage. The optimization resulted in an unusual mixed-flow compressor design with very low aspect ratio blades and a high rotational speed of up to 60,000 rpm. Due to the unusual design, experimental validation of the performance predictions by means of CFD is necessary. This paper presents the first experimental results obtained using a preliminary prototype at part-speed, i.e. rotational speeds from 20,000 to 30,000 rpm. The experimentally-determined pressure ratios deviate up to 1.5 %, the polytropic efficiencies up to 4 percentage points from the CFD predictions. Besides the deficiencies of available turbulence models, the underestimation of overall losses is presumably due to the omission of the volute in the CFD model. An experimental validation of the CFD predictions at full-speed is under way.

1. Introduction

Improved high-lift systems have the potential to reduce noise and carbon dioxide emissions of modern commercial aircraft. An efficient active high-lift system using a flexible leading-edge device, together with a combination of boundary layer suction and blowing over a Coanda flap was presented by Radespiel and Heinze [1]. The required air supply for this system is provided by compact electrical compressor units, which are integrated into the wings. A design process for the components of these compressor units was developed by Teichel et al. [2]. Components with high specific power are needed to reduce mass and volume of the system. The use of automatic optimization methods as described by Teichel et al. [3] resulted in an unusual, transonic, mixed-flow compressor design with a high axial flow component. According to CFD predictions, the aerodynamic design point (total pressure ratio of 2.33 and corrected mass flow rate of 1.11 kg/s) is reached at a corrected rotational speed of 60,125 rpm with a polytropic efficiency of 83.3 %. The impact of inlet flow distortion on the stage performance resulting from an integration of the electrical components into the compressor inlet duct was investigated by Kauth et al. [4]. Figure 1 shows the compressor test rig, which was used for the experimental part-speed validation of the present study [5].

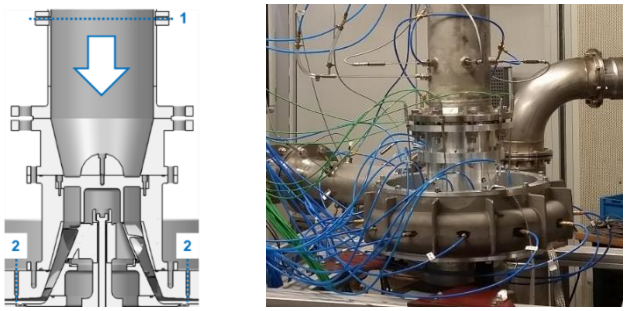

Figure 1. Left: longitudinal section of the compressor as tested, with performance measurement stations '1' in inlet duct and '2' in radial duct upstream of the volute; right: compressor test facility [5].

Mixed-flow compressors combine advantages of both axial and radial compressors, resulting in compact stages with high specific power. Most known mixed-flow compressor designs are similar to centrifugal compressors with a high impeller hub cone angle. Watanabe & Sakai [6] showed an improvement of the total and static pressure ratio for decreasing cone angles. Diener et al. [7] combined a neural network with CFD computations in order to optimize the aerodynamic design of a mixed-flow compressor, followed by mechanical analyses. For initial design considerations Hazby et al. [8] and Nassar et al. [9] made use of a simpler streamline curvature solver, before analysing the design using CFD. Additionally, Hazby et al. [8] compared the predicted performance to experimental results, showing good agreements for low-speed operation. However, in particular for higher mass flow rates, lower total pressure ratios were predicted. In contrast, mixed-flow compressors with a high axial flow component have rarely been discussed in open literature. A detailed design description and experimental characterisation of such a transonic mixed-flow compressor was given by Musgrave & Plehn [10]. The stage with a pressure ratio of 3:1 was designed to run downstream of an axial compressor stage. Experimental and analytical investigations of a supersonic mixed-flow compressor were done by Mönig et al. [10].

The performance and stability of any type of compressor can be strongly influenced by the tip leakage flow. For axial compressors the tip clearance effects are mainly determined by the clearance-to-blade-height ratio according to Storer & Cumpsty [12]. Due to the small blade heights, the magnitude of this effect is relatively high for mixed-flow compressors. However, only few works were published on this subject. An experimental study of tip clearance effects for a mixed-flow compressor with a high proportion of radial flow was performed by Rajakuma et al. [13] for constant and variable tip clearance gaps. Numakura et al. [14] conducted a detailed numerical and experimental investigation of the casing treatment of two mixed flow compressors. For the present compressor an axial slot casing treatment has been designed by Du & Seume [15] and recently experimentally evaluated by Du et al. [16].

2. Numerical and experimental methods

2.1. Computational fluid dynamics

The industrial CFD code TRACE (version 8) was used for the numerical performance predictions. The governing equations in TRACE are discretized by means of the finite volume method, time discretization uses an implicit first-order Euler method and the solver uses a predictor-corrector algorithm [17]. TRACE was verified for turbomachinery applications e.g. in [18]. The SST turbulence model was applied with the assumption of a fully-turbulent flow. All walls were set as adiabatic with a non-slip condition. A low-Reynolds number approach was used, and consequently all meshes used a dimensionless wall distance of $y^+ \approx 1$ to ensure that the first grid node was situated within the viscous sublayer of the boundary layer. All simulations used the same inlet boundary conditions: total pressure 101,350 Pa, total temperature 288.15 K, radial and tangential flow angle 0°, turbulent intensity 5 %, and turbulent length scale 18.8 µm. At the outlet, an average static pressure between 102,000 and 130,000 Pa was imposed at mid-span. Interfaces between rotating and stationary domains were modelled using the mixing-plane approach. A rotational speed between 20,000 and 30,000 rpm was imposed on the fluid in the rotor domain. To compute the characteristic compressor speed lines, the static pressure at the outlet was increased incrementally for each rotational speed, using the previous converged solution

as initial condition. A solution was considered as converged if the root mean square residuals decreased to 10^{-5}, and the maximum residuals to 10^{-3}. Additionally, mass flow, pressure ratio, efficiency and maximum eddy viscosity were monitored and not allowed to vary more than 0.01 % over the last 100 iterations. The CFD simulations during the optimized design process described in [3] had been done using only a model of the rotor and stator row without any connecting ducts [2]. To validate the CFD simulations, the numerical model should match the experimental setup as well as possible. Consequently, new grids were generated for the blade rows, which had to be manufactured with larger leading and trailing edge radii than anticipated. Different rotor tip clearances between 0.1 and 0.4 mm were modelled, while the stator tip clearance was fixed to 0.1 mm. Additionally, the inlet and outlet ducts of the stage, where pressure and temperature were measured in the experiment, were included into the model. Structured grids were generated for rotor, stator and inlet duct using NUMECA AutoGrid5. The structured grid of the radial outlet duct was generated with ANSYS ICEM CFD.

A grid convergence study according to [19] was performed for the key variable polytropic efficiency on three grids of increasing resolution at a high Reynolds number operating point. The fine grid convergence index GCI_1 was calculated using Eq. 1 with the approximated relative error according to Eq. 2, with f_i being the solution on grid level i. The grid refinement factors were $r_{21} = 1.45$ and $r_{32} = 1.36$. An empirical safety factor of $F_S = 1.25$ was used, as suggested by [20]. The apparent order was calculated using Eq. 3, where $s = sgn((f_3 - f_2)/(f_2 - f_1))$. Due to its reasonable trade-off between computational cost and accuracy, the medium grid ($GCI_2 = 0.0011$) was chosen for the numerical performance analysis.

$$GCI_1 = \frac{F_S e_{21}}{r_{21}^p - 1} \tag{1}$$

$$e_{21} = \left| \frac{f_1 - f_2}{f_1} \right| \tag{2}$$

$$p = \frac{\ln\left|\frac{f_3 - f_2}{f_2 - f_1}\right| + \ln\left(\frac{r_{21}^p - s}{r_{32}^p - s}\right)}{\ln(r_{21})} \tag{3}$$

2.2. Experiment

Experimental validation of the numerical performance predictions is necessary in particular because of the unconventional compressor design. As the whole design process of the electrically-powered high-lift system relies on these performance predictions, first results were required before the newly developed full-speed electrical machine was available. Therefore as a first step, part-speed tests were conducted using a commercially available electric motor with a maximum rotational speed of 30,000 rpm. The inlet flow direction was axial and downstream of the stator the flow was guided to the radial direction and into a volute, due to the bigger diameter of this motor, compared to the future full-speed motor.

The rotor tip clearance was varied by using distance washers of varying thicknesses between the rotor and the stator casing. The nominal tip clearances used during the experiments were the “Design clearance” of 0.1 mm and the “Large clearance” of 0.2 mm. Due to manufacturing tolerances a constant stator tip clearance of 0.1 mm was unavoidable. To evaluate the compressor performance, static pressure taps and total temperature probes were used at the inlet and outlet of the compressor rig (see Figure 1), as well as in the radial duct between stator and volute. Inflow dynamic pressure was measured using a Prandtl tube. Pressures were measured relative to the ambient pressure, which was recorded separately. An ultrasonic gas flow meter was used to measure the air volume flow. All variables were recorded using a sampling rate of 5 Hz with 20 samples for every operating point. Three parallel throttle valves were used to control the compressor back pressure. Table 1 summarizes the information about all measurement devices.

Table 1. Instrumentation of the test rig

Location	Transducer	Range	Accuracy
Measuring cabin	Mensor CPT6100	55.2 to 117.2 kPa	0.01 %
Air intake	FlowSIC 600	20 to 30000 m³/h	1 %
Inlet duct	NetScanner 9116	15 psi	0.05 % FS
	PT100	-100 to 450 °C	0.15 + 0.002 |t| °C
Radial duct	NetScanner 9816	45 psi	0.05 % FS
	Type K thermocouple	-40 to 1000 °C	1.5 °C
Outlet duct	NetScanner 9116	45 psi	0.05 % FS
	PT100	-100 to 450 °C	0.15 + 0.002 |t| °C

For each performance parameter $y = f(x_1, \dots, x_m)$, the resulting measurement uncertainty was quantified according to [21] using Eq. 4. Assuming a Student's t-distribution, the random uncertainty of each measurand x_i was calculated based on its experimental standard deviation for a 90 % confidence interval (CI). The systematic uncertainty of each measurand was calculated from the accuracy of the transducer, assuming a uniform distribution.

$$u(y) = \sqrt{\sum_{i=1}^{m} \left(\frac{\delta f}{\delta x_i}\right)^2 u^2(x_i)} \tag{4}$$

In the following, measurement results are given as arithmetic mean values together with the calculated standard uncertainty. The main compressor performance parameters used for the validation are static and total pressure ratio, as well as polytropic efficiency. While the static pressure ratio $\Pi = p_{out}/p_{in}$ can be calculated directly from the measured static pressures at inlet and outlet, the total pressure at the outlet has to be calculated using Eq. 5 to 7. The polytropic compressor efficiency is calculated according to Eq. 8.

$$p_t = p\left(\frac{T_t}{T}\right)^{\frac{\kappa}{\kappa-1}} \tag{5}$$

$$T = T_t - \frac{c_x^2}{2c_p} \tag{6}$$

$$c_x = \frac{\dot{m}RT}{pA} \tag{7}$$

$$\eta_p = \frac{\kappa-1}{\kappa} \frac{ln\left(\frac{p_{t,2}}{p_{t,1}}\right)}{ln\left(\frac{T_{t,2}}{T_{t,1}}\right)} \tag{8}$$

For the performance comparison, the rotational speed N and the measured mass flow rate $\dot{m}$ are corrected using inlet pressure and temperature, as well as the international standard atmosphere (p_{ref} = 101,325 Pa and T_{ref} = 288.15 K) [22].

$$\dot{m}_{corr} = \dot{m} \frac{p_{ref}}{p_{t,1}} \sqrt{\frac{T_{t,1}}{T_{ref}}} \tag{9}$$

$$\mathrm{N}_{corr} = \mathrm{N} \sqrt{\frac{T_{ref}}{T_{t,1}}} \tag{10}$$

2.3. Finite Element Analysis

The compressor geometry changes during operation due to centrifugal forces and thermal expansion. To estimate the appropriate "hot" geometry, a finite element analysis (FEA) was performed using ANSYS Workbench. For this purpose, wall temperatures and pressures at different operating points were extracted from the CFD results and mapped on the FEA grids of rotor and casing. The maximum calculated overall deformation of the rotor blades for the operating point with the highest temperatures and pressures at 30,000 rpm is 0.06 mm. An evaluation of the radial component of rotor tip and casing

displacement yields a mean rotor tip clearance increase of 0.009 mm at that operating point. It is assumed that the effect on the subsonic compressor performance due to those small changes in clearance and blade profile shape can be neglected. For this reason, the "cold" geometry was used for the CFD analysis presented in this paper. However, this assumption will not be valid at higher rotational speeds for two reasons. First, the deformations will become more severe due to higher centrifugal forces and temperatures. Moreover, the locally supersonic flow regime on the suction side at high-speed operating points is more sensitive to changes in blade profile geometry [22].

3. Results

As described before, compressor outlet pressures and temperatures were measured at two stations – upstream and downstream of the volute. Performance parameters calculated with the measurements upstream of the volute are denoted with "stage", those calculated with the downstream measurements with "overall rig". Figure 2 presents a comparison of both performance calculations at design tip clearance. Due to the use of thermocouples instead of PT100 at the measurement station upstream of the volute, the resulting uncertainties are higher for the "stage" performance. As can be seen in Figure 2, the volute seems to cause substantial pressure losses, most severely at high mass flow rates. The reason for this is probably a mismatch of stage and volute, as the latter is part of the test rig and has not been designed for the mixed-flow compressor. As the performance of the volute is not of interest for the present study, all following evaluations are done using the "stage" performance. \

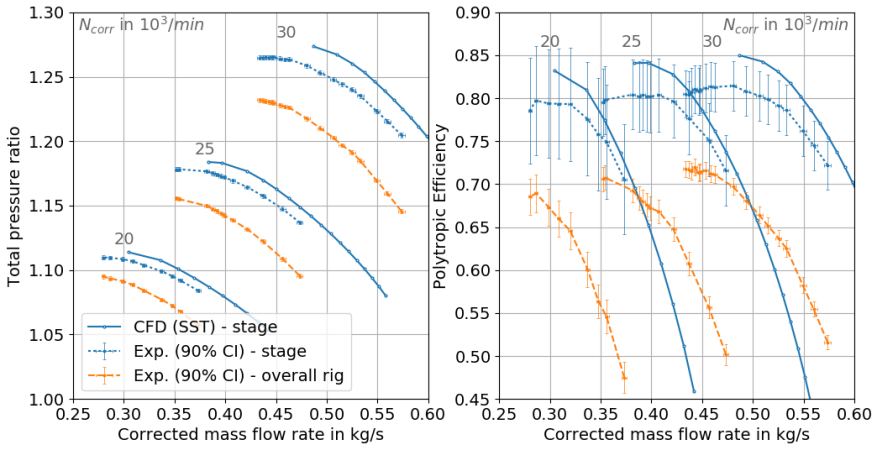

Figure 2. Compressor performance (design tip clearance) for different outlet measurement positions.

The predicted stage performance at design tip clearance is also shown in Figure 2. While the measured static pressure ratios (not shown) match the prediction within less than 1 %, the total pressure ratios deviate up to 1.5 %, and the polytropic efficiencies up to 4 percentage points. The total pressure ratio offset is almost constant over most of the operating range and gets smaller near peak efficiency. Moreover, the deviations increase at higher rotational speeds. The experimentally determined stability limit was observed at lower corrected mass flow rates compared to the last converged CFD solution for every rotational speed. Deviations in the same order of magnitude between CFD predictions and performance measurements of a mixed-flow compressor were observed by [8]. They used the k-ε turbulence model for their CFD predictions, and presumed that the deviations were due to turbulence modelling and geometrical differences between numerical model and experiment.

As there is no clear reason to mistrust the measurement data, the most likely reason for the difference between numerical and experimental results is omitting the volute of the test rig in the CFD model. This could cause a deviation in the results, as a volute imposes a non-axisymmetrical pressure field on the stage upstream [22]. Another feature of the test rig, which could not be modelled and has a potentially detrimental effect on the performance, is the axial thrust compensation system of the compressor [5]. A labyrinth seal is used to minimize the leakage through the rotor hub, but its effectiveness could not be verified yet.

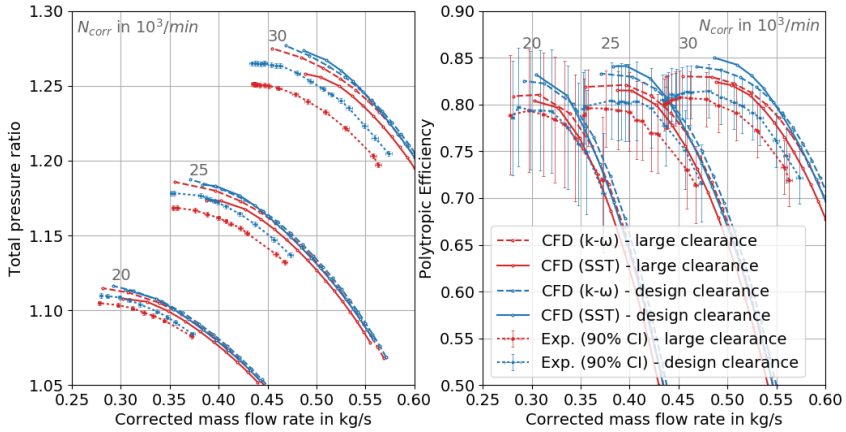

Figure 3. CFD performance prediction using different turbulence models for two tip clearance settings.

The mixed-flow compressor investigated here has a unique design and due to its compactness, "secondary" flow phenomena and associated losses are expected to be more dominant than in bigger axial compressors. An important source of modelling errors in RANS computations is the use of turbulence models [23]. To demonstrate the sensitivity of the CFD results to the choice of turbulence model, Figure 3 presents results obtained using two of the most commonly used turbulence models for compressor simulations, the SST and the k-ω model. As explained by [23], turbulence models usually give good results for fully turbulent and attached boundary layers. However, especially for compressors near stall, where separating and separated flows occur, big differences between turbulence models can be expected. Figure 3 confirms this hypothesis, as the biggest differences between the two models occur near the stability limit.

For the design tip clearance, both turbulence models give similar results, although the efficiency from the k-ω model is slightly closer to the experimental results. With increasing tip clearance the total pressure ratio decreases, while the impact increases with higher rotor speeds. As mentioned by [13], the effect of tip clearance is influenced by factors like geometry and flow field, and therefore not linearly correlated with the speed. When comparing the numerical results of both tip clearance settings, the k-ω model seems to be less sensitive to a change in tip clearance compared to both experimental as well as SST results. A parameter study was performed with different tip clearances to further evaluate this phenomenon. Figure 4 shows the results for the maximum total pressure ratio and maximum polytropic efficiency at two different rotational speeds. When using the SST model, the detrimental effect of an increased rotor tip clearance on compressor performance is more severe compared to the predictions using the k-ω model.

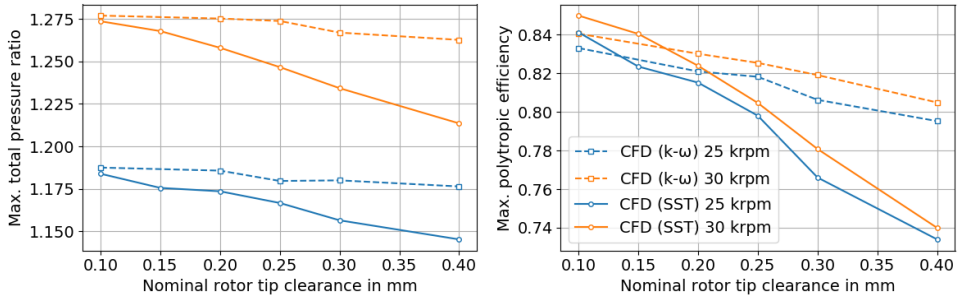

Figure 4. Effect of turbulence model, rotational speed, and rotor tip clearance on maximum performance.

4. Conclusions

An experimental part-speed validation was performed for a newly designed mixed-flow compressor for an active high-lift system at 20,000 to 30,000 rpm. For this speed range, it was demonstrated that using the "cold" geometry for the CFD analysis is acceptable. An upstream effect of the volute, which was omitted in the current CFD model, is the most likely reason for the deviations of the measured stage performance to the CFD predictions in terms of total pressure ratio and polytropic efficiency. The

numerical stability limit was demonstrated to be a conservative criterion for the compressor stall limit. The next step will be to include the volute into the CFD model and to estimate the leakage flow through the labyrinth seal of the axial thrust compensation system. Moreover, the appropriate "hot" geometry will be used for the CFD analysis in the context of the planned full-speed validation.

It was shown that the CFD results of this mixed-flow compressor are sensible to the choice of turbulence model, depending on tip clearance and rotational speed. As no detailed flow measurements were done yet, it was not possible to evaluate whether local flow phenomena, e.g. separation, were correctly modelled. For this reason, it is planned to investigate the detailed flow structure in the future, e.g. by means of particle image velocimetry. Further experiments using a newly developed high-speed electrical machine to validate the performance predictions and the correction method in the transonic range from 40,000 to 60,000 rpm are under way.

Acknowledgements
The authors would like to thank the German Research Foundation (DFG) for supporting this fundamental research in active high-lift systems for future aircraft as part of the Collaborative Research Centre 880 (Sonderforschungsbereich SFB 880). Moreover, the authors thank the German Aerospace Center (DLR) for the permission to use the solver TRACE.

References

[1] Radespiel R and Heinze W 2014 SFB 880: fundamentals of high lift for future commercial aircraft*CEAS Aeronautical J.* **5**
[2] Teichel S H, Dörbaum M, Misir O, Merkert A, Mertens A, Seume J.R, Ponick B 2015 Design Considerations for the Components of Electrically Powered Active High-lift Systems in Civil Aircraft, *CEAS Aeronautical J.* **6**
[3] Teichel S H, Verstraete T, Seume J R 2017 Optimized Multidisciplinary Design of a Small Transonic Compressor for Active High-Lift Systems *JGPP* **9**
[4] Kauth F, Narjes G, Müller J K, Mertens A, Ponick B, Seume J R 2018 Electrically driven, Compact, Transonic Mixed-Flow Compressor for Active High-Lift Systems in Future Aircraft, *Proceedings of GPPS Forum* **18**
[5] Kauth F, Narjes G, Müller J, Ponick B, Mertens A, Seume J.R 2017 Compact Electrical Compressors for Active Flow Control in Autonomous High-Lift Systems, SFB 880 – Fundamentals of High-Lift for Future Civil Aircraft: Biennial Report (TU Braunschweig – Campus Forschungsflughafen, Braunschweig, 2017)
[6] Watanabe I, Sakai T 1965 Effect of the Cone Angle of the Impeller Hub of the Mixed Flow Compressor upon Performance Characteristics *SAE Technical Paper* **650037**
[7] Diener O H F, van der Spuy S J, von Backström T.W, Hildebrandt T 2016 Multi-Disciplinary Optimization of a Mixed-Flow Compressor Impeller *Proceedings of ASME Turbo Expo 2016*
[8] Hazby H, Casey M, Numakura R, Tamaki H 2015 A Transonic Mixed Flow Compressor for an Extreme Duty, *ASME. J. Turbomach.*
[9] Nassar A, Giri G, Moroz L, Sherbina A and Klimov I 2016 Design and Analysis of a High Pressure Ratio Mixed Flow Compressor Stage, 52nd AIAA/SAE/ASEE Joint Propulsion Conference, AIAA Propulsion and Energy Forum (2016)
[10] Musgrave D S, Plehn N J 1987 Mixed-Flow Compressor Stage Design and Test Results With a Pressure Ratio of 3:1 *ASME. J. Turbomach*
[11] Mönig R, Elmendorf W, Gallus H E 1993 Design and Rotor Performance of a 5:1 Mixed-Flow Supersonic Compressor *ASME. J. Turbomach* **115**, 3
[12] Storer J A, Cumpsty N A 1994 An Approximate Analysis and Prediction Method for Tip Clearance Loss in Axial Compressors *ASME. J. Turbomach* **116**, 4
[13] Rajakumar D R, Ramamurthy S, Govardhan M 2015 Experimental investigations on effects of tip clearance in mixed-flow compressor performance *Proceedings of the Institution of Mechanical Engineers, Part G: Journal of Aerospace Engineering* **229** 5
[14] Numakura R, Tamaki H, Hazby H, Casey M 2014 Effect of a Recirculation Device on the Performance of Transonic Mixed Flow Compressors *Proceedings of ASME Turbo Expo 2014*

[15] Du J, Seume J R 2017 Design of Casing Treatment on a Mixed-Flow Compressor. *Proceedings of ASME Turbo Expo* 2017
[16] Du J, Li J, Zhang Q, Kauth F, Seume J R 2019 Experimental Study on the Influence of Casing Treatment on Near-Stall Unsteady Behavior of a Mixed-Flow Compressor. *Proceedings of ASME Turbo Expo 2019*, to be published
[17] Deutsches Zentrum für Luft- und Raumfahrt, *TRACE User Guide*, http://www.trace-portal.de/userguide/trace/index.html (accessed March 2019)
[18] Kügeler E, Nürnberger D, Weber A, Engel K 2008 Influence of blade fillets on the performance of a 15 stage gas turbine compressor, Proceedings of ASME Turbo Expo 2008
[19] American Society of Mechanical Engineers, Standard for verification and validation in computational fluid dynamics and heat transfer (American Society of Mechanical Engineers, New York, 2009)
[20] Roache P J 1998 Verification and Validation in Computational Science and Engineering (Hermosapublishers, Albuquerque, 1998)
[21] DIN 1319-3:1996-05 1996Fundamentals of metrology - Part 3: Evaluation of measurements of a single measurand, measurement uncertainty
[22] Cumpsty N A 2004 Compressor aerodynamics (Krieger Pub, Malabar, Fla, 2nd ed, 2004)
[23] Denton J D 2010 Some limitations of turbomachinery CFD, Proceedings of ASME Turbo Expo 2010